# Optical Engineering

Optical Engineering. SPIED igital Library.org

## Thermal stabilization of a fiber-based channeled spectropolarimetry

Ali Altaqui Michael W. Kudenov



### Thermal stabilization of a fiber-based channeled spectropolarimetry

#### Ali Altaqui\* and Michael W. Kudenov

North Carolina State University, Department of Electrical and Computer Engineering, Optical Sensing Laboratory, Raleigh, North Carolina, United States

**Abstract.** Channeled spectropolarimetry (CSP) is a spectral modulation technique that furnishes snapshot polarimetric measurements. Among the different spectropolarimetric methods, fiber-based techniques are fundamental requirements in specific biomedical procedures, such as endoscopy. However, the optical fiber exhibits high sensitivity to temperature changes, which subsequently incurs errors in the polarimetric reconstructions. We present a calibration technique for fiber-based CSP that leverages phase-shifting interferometry (PSI) to acquire and demodulate the fiber's retardation phase accurately. This technique provides high robustness against temperature variations and improved polarimetric reconstruction performance. Experimental results demonstrated that the PSI calibrations offer higher stability and accuracy, at different optical fiber temperatures, as compared to reference-beam calibrations. © 2019 Society of Photo-Optical Instrumentation Engineers (SPIE) [DOI: 10.1117/1.OE.58.12.124102]

Keywords: spectropolarimetry; optical fiber; spectroscopy; polarimetry; optical metrology.

Paper 191430 received Oct. 15, 2019; accepted for publication Nov. 21, 2019; published online Dec. 5, 2019.

#### 1 Introduction

Channeled spectropolarimetry (CSP) is a technique based on spectral polarization modulation of light that enables snapshot measurements of the Stokes parameters. This technique is particularly important in various remote sensing applications that require time-resolved spectropolarimetric measurements.<sup>2,3</sup> In addition, CSP is suitable in situations where the polarization information cannot be modulated in the spatial or temporal dimension and where the sensor device is highly responsive to the spectral contents of light.<sup>4</sup> The majority of the previously reported work on CSP focuses on the use of birefringent crystal retarders to provide spectral modulations of the Stokes parameters. 5-10 In some cases, it is desirable to use optical fibers instead of crystal retarders, especially in endoscopic applications that require spectropolarimetry to improve the diagnostic performance, 11–13 for example, in-vivo inner tissue characterizations for early disease diagnostics. 14,15 Another future application of fiber-based CSP can be realized in full- or partial-Mueller matrix (MM) CSP systems for more accurate polarization bidirectional reflectance distribution function (BRDF) measurements. 16,17 In these systems, the use of fiber bundles in the polarization analyzer can potentially enable higher angular and temporal resolutions, as well as wider angular coverage due to their flexibility as compared to rigid crystal retarders. One major issue, relating to the use of optical fiber in spectropolarimetry, is the fiber's high sensitivity to environmental perturbations, such as temperature. 18 This issue causes errors and uncertainty in the polarimetric reconstructions of light. One of the most notable work in fiber-based CSP has been reported in Ref. 19; however, it does not address nor provide a solution to the fiber's sensitivity to variations in temperature.

We have recently reported a CSP technique, which utilized the concept of phase-shifting interferometry (PSI) to offer robustness against environmental changes and to provide high-accuracy Stokes parameter reconstructions. The PSI algorithm requires a minimum of three unique intensity measurements in order to accurately determine the retardation phase—a feature that does not exist in other calibration methods, such as the reference-beam and the self-calibration techniques. It should be noted that our previous PSI-based CSP system was based on the use of crystal retarders rather than optical fibers. In addition, it was primarily focused on comparing the PSI method to that of the self-calibration at room temperature and did not test the CSP performance at different temperatures.

In this paper, we implement the PSI calibration method in a fiber-based CSP system and experimentally show its performance at different temperatures. In addition, we compare the performance of the PSI technique to that of the reference-beam method at fiber temperatures of 20°C, 35°C, 40°C, 45°C, and 50°C. Experimental results reveal that the PSI calibration method displays a more robust performance against temperature variations and a higher Stokes reconstruction accuracy, as compared to the reference-beam calibration technique. This paper is organized as follows. Section 2 provides the theoretical system model of the PSI fiber-based CSP structure. Section 3 describes our experimental setup and the different procedures taken during the experiments. Finally, Sec. 4 presents our experimental results.

#### 2 Theoretical System Model

Figure 1 depicts the structure of the fiber-based channeled spectropolarimeter. The input consisted of a broadband optical source and a polarization state generator (PSG), which generated the input Stokes parameters, defined as

0091-3286/2019/\$28.00 © 2019 SPIE

<sup>\*</sup>Address all correspondence to Ali Altaqui, E-mail: aaaltaqu@ncsu.edu

Fig. 1 The basic setup of the fiber-based channeled spectropolarimeter.

$$S(\sigma) = \begin{bmatrix} S_0(\sigma) \\ S_1(\sigma) \\ S_2(\sigma) \\ S_3(\sigma) \end{bmatrix} = \begin{bmatrix} I_0 + I_{90} \\ I_0 - I_{90} \\ I_{45} - I_{135} \\ I_R - I_L \end{bmatrix}, \tag{1}$$

where  $\sigma$  is the wavenumber  $(\lambda^{-1})$ ,  $S_0$  is the light's intensity,  $S_1$  is the difference between horizontal and vertical linear polarization states,  $S_2$  is the difference between +45 deg and -45 deg linear polarization states, and  $S_3$  is the difference between right and left circular polarization states. The generated polarized light passes through an achromatic quarter-wave plate (AQWP) with its fast axes oriented at 0 deg relative to the horizontal. This enabled full linear spectral modulation of the Stokes parameters  $(S_1 \text{ and } S_2)$ , as opposed to conventional single-retarder CSP system, where  $S_1$  and  $S_3$  are spectrally modulated.<sup>22</sup> The light is then focused onto a single-mode polarization-maintaining (PM) fiber,<sup>23</sup> with its fast axis oriented at 45 deg. As light propagates through the PM fiber, both  $S_1$  and  $S_2$  are modulated onto the fiber spectral carrier frequency  $\varphi(\sigma)$ , which is defined as

$$\varphi(\sigma) = 2\pi\sigma LB(\sigma),\tag{2}$$

where L is the optical fiber length and  $B(\sigma) = |n_e(\sigma) - n_o(\sigma)|$  is the fiber's birefringence, and  $n_e$  and  $n_o$  are the fiber's extraordinary and ordinary refractive indices, respectively.

After exiting the PM fiber, the modulated light traverses a polarization phase shifter, which consisted of an AQWP and an analyzer oriented at an angle  $\theta$  from the horizontal. The analyzer's orientation angle dictates the amount by which the fiber spectral carrier frequency is phase-shifted. Setting the analyzer to an angle of  $\theta$  creates a phase shift in the spectral

carrier frequency by  $2\theta$ .<sup>24</sup> The intensity spectrum at the output of the analyzer is given as

$$I_{\theta}(\sigma) = \frac{1}{2} [S_0(\sigma) + S_1(\sigma) \{\cos(\varphi)\cos(2\theta) + \sin(\varphi)\sin(2\theta)\}$$
  
+  $S_2(\sigma) \{\sin(\varphi)\cos(2\theta) - \cos(\varphi)\sin(2\theta)\}].$  (3)

Inverse Fourier transformation of the intensity spectrum yields an interferogram that contains three distinct channels as a function of the optical path difference (OPD)  $\Delta z$ . The intensity spectrum's Fourier transformation is given as

$$J_{\theta}(\Delta z) \propto \frac{S_0(\Delta z)}{2} * \delta(\Delta z) + \frac{S_{12}(\Delta z)}{4} * [\delta(\Delta z - BL)e^{j2\theta}] + \frac{\overline{S_{12}}(\Delta z)}{4} * [\delta(\Delta z + BL)e^{-j2\theta}], \tag{4}$$

where  $\delta$  is defined as the Dirac delta function,  $S_{12} = S_1 + jS_2$  is the complex linear Stokes parameter,  $\overline{S}_{12}$  is the complex conjugate of the linear Stokes parameter, and \* denotes a convolution. Figure 2 displays the three spectral channels in the Fourier domain for a fiber length of L=30 cm, fiber birefringence of  $5\times 10^{-4}$  (achromatic), wavelength integration range from 0.3 to 2  $\mu$ m, and an analyzer oriented at 0 deg. The center-burst channel  $(C_0)$  contains  $S_0$ , whereas channel 1  $(C_1)$  and its conjugate  $(C_{-1})$  contains  $S_{12}$  and  $\overline{S}_{12}$ , respectively.

The four-step PSI calibration method<sup>25</sup> was used to reconstruct  $S_1$  and  $S_2$ . This was achieved by first applying a bandpass filter to both the channel and its conjugate,  $C_1$  and  $C_{-1}$ , respectively, followed by forward Fourier transform. The resulting intensity spectrum is given as

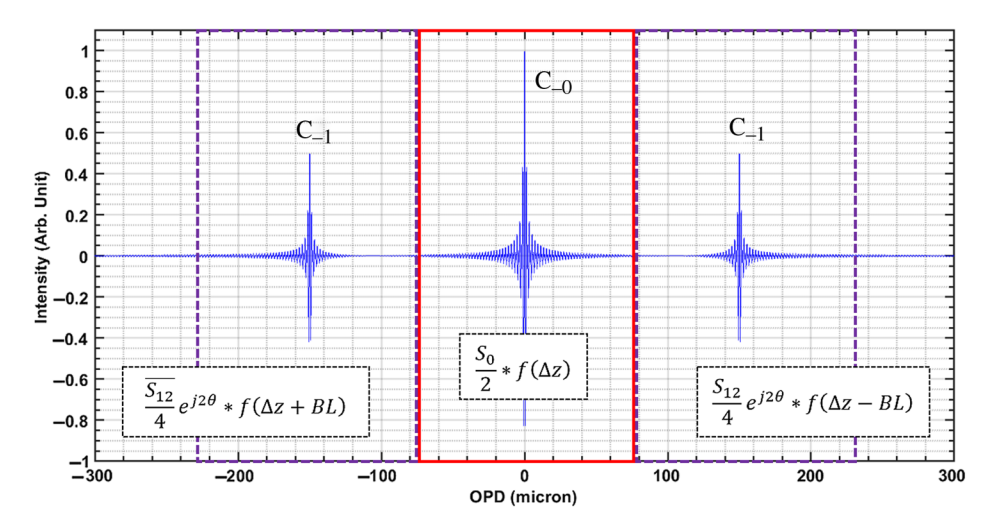


Fig. 2 The intensity spectrum's Fourier transformation in the OPD domain.

$$\Im(C_{\pm 1}) = I_{\theta}(C_{\pm 1}) = \frac{S_{12}(\sigma)}{4} \left[ e^{-j\varphi} e^{j2\theta} + e^{j\varphi} e^{-j2\theta} \right]. \tag{5}$$

Second, we determined the intensity spectrum in Eq. (5) at four different polarization analyzer orientations of 0 deg, 45 deg, 90 deg, and 135 deg. The phase  $\varphi$  can now be determined by applying the four-step PSI algorithm, which is given as

$$\tan(\varphi) = \frac{I_{135} - I_{45}}{I_0 - I_{90}},\tag{6}$$

where  $I_0$ ,  $I_{45}$ ,  $I_{90}$ , and  $I_{135}$  represent the spectral-domain intensity measurements, taken at analyzer orientations of 0 deg, 45 deg, 90 deg, and 135 deg, respectively. Using Eq. (6), the fiber's phase is calculated as

$$\varphi = \tan^{-1} \left[ \frac{-2je^{j\varphi} + 2je^{-j\varphi}}{2 e^{j\varphi} + 2 e^{-j\varphi}} \right]. \tag{7}$$

Accordingly,  $S_{12}$  can be determined by dividing the filtered right sideband of  $C_1$ , that is,  $I_0(C_{+1})$ , by the phase exponential  $e^{j\varphi}$ . Finally,  $S_1$  and  $S_2$  can be acquired by taking the real and imaginary parts of  $S_{12}$ , respectively. Note that channel cross talk between  $C_0$  and  $C_{\pm 1}$  can also be minimized, as part of the PSI calibration process. This is achieved by adopting the dual-scan approach, reported in Ref. 26, which is based on adding and subtracting the intensities  $I_0$  and  $I_{90}$ . The PSI calibration method, as well as the dual-scan approach, will be experimentally used in our fiber-based channeled spectropolarimeter structure to reconstruct the Stokes parameters at different optical fiber temperatures.

#### 3 Experimental Setup and Procedures

Experiments were conducted to test the proof of principle of the PSI calibration technique in the fiber-based channeled spectropolarimeter under different temperatures. Figure 3 depicts the experimental setup. A light-emitting diode (LED) was used at the input of the system, with an intensity spectrum as depicted in Fig. 4. Two lenses (L1 and L2) were used to relay the light to the optical fiber. Both lenses have a diameter of 25 mm and a focal length of 100 mm. The first lens (L1) was used to collimate the LED light, whereas the second lens (L2) was used to focus the light within the numerical aperture (NA) of the optical fiber. A wire-grid polarizer was placed in front of the second lens to generate different polarization states. In addition, a Fresnel rhomb (FR), which

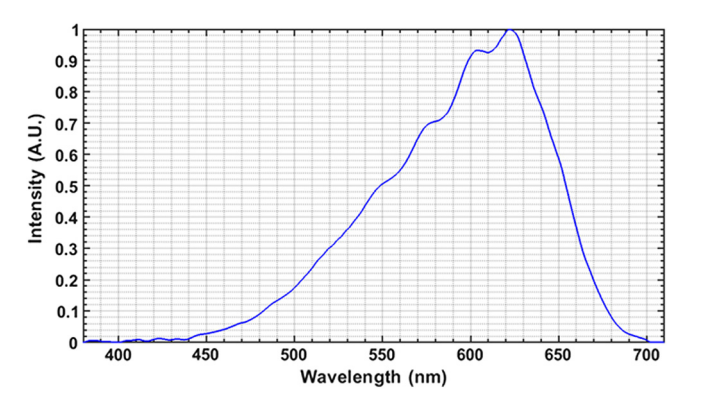


Fig. 4 LED spectrum.

functions as an AQWP, was placed just before the entrance of the optical fiber in order to provide full linear Stokes modulation. Note that a better experimental setup could have been realized by placing L2 between the FR and the optical fiber. In that way, the beam incident on the FR would be collimated rather than converging, and hence FR would produce a more stable 90-deg retardance. However, the setup of L2 and FR was governed by the low NA of the fiber. In addition, we noticed that placing L2 after the FR yielded optical cross talk between the modulated light from the FR and the background unmodulated LED light. This issue can be solved by using AOWP film instead of FR. The optical fiber, used in the experiment, was a single-mode PM fiber from Thorlabs, Inc. (PM460-HP), with a spectral bandwidth of 460 to 700 nm, NA of 0.12, a length of 30 cm, and a birefringence that ranges from 0.0003 to 0.0005 at the fiber spectral range. Moreover, the optical fiber was placed inside a cylindrical tube, which acts as a temperature chamber, with electrical wires uniformly coiled around its outer surface. The temperature inside the tube was controlled via a thermoelectric temperature controller (TC-48-20) from TE technology. The polarization phase shifter, which is composed of an AOWP and a polarization analyzer, was placed at the output of the fiber, followed by a dispersive spectrometer consisting of a Fresnel prism and a focal plane array (FPA). The FPA contains a camera (BFLY-U3-13S2M-CS) from FLIR Systems, Inc., and a Nikon lens (AF NIKKOR 50mm f/1.8D). Note that, unlike Fourier transform spectrometers, which can display the channeled intensity spectrum directly in the Fourier domain, dispersive spectrometers display the intensity spectrum in the spectral domain. Therefore, Fourier transformation is typically required in

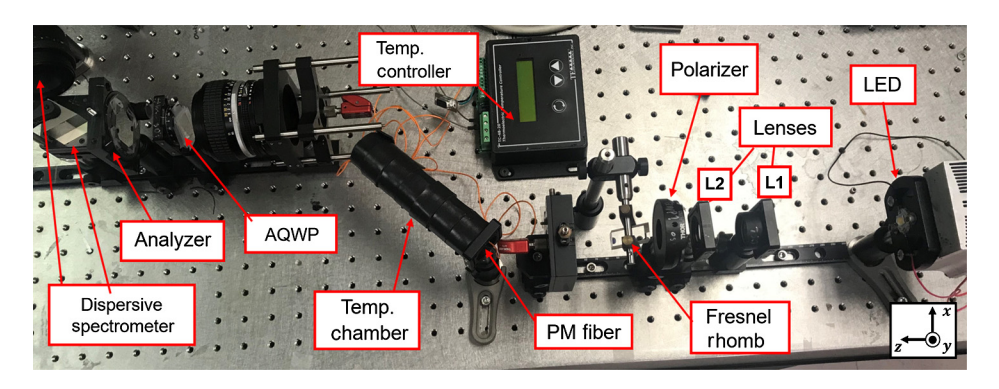


Fig. 3 Experimental setup of the fiber-based channeled spectropolarimeter.

dispersive-based CSPs. Nevertheless, as far as the PSI algorithm in Eq. (6) is concerned, it can be applied to either the spectral domain or its Fourier counterpart, provided that all intensity measurements are collected in the same domain. Also, it should be mentioned that the length of the PM fiber, used in the experiment, was limited by the size of our temperature chamber; however, greater lengths of fiber can be used with similar performance.

The experimental procedures were conducted as follows. (1) The FPA camera pixels were calibrated and mapped to wavelengths using neon and xenon gas discharge lamps. (2) The fast/slow axes of the optical fiber were determined using a common retarder characterization technique in which the optical fiber was placed between two parallel polarizers. The fiber's fast axis was then set to 45 deg relative to the positive x axis. (3) The temperature of the fiber was varied from 20°C to 50°C in 5°C increments. (4) For a specific PSG orientation and temperature, intensity measurements were collected for analyzer orientations of 0 deg (positive x axis), 45 deg, 90 deg (positive y axis), and 135 deg. Note that the time duration for collecting all the four intensity measurements can take  $\sim 15$  s. To further improve this temporal scanning, one can use the three-step PSI algorithm provided in Ref. 25. Alternatively, for some applications that are susceptible to errors due to temporal factors, one can utilize division of amplitude or division of focal plane polarimetry to collect those four intensity measurements at once. (5) The polarization sensitivity of the dispersive spectrometer was negated by characterizing its response to input polarization of  $\theta =$ 0 deg, 45 deg, 90 deg, and 135 deg. This ensured an identical response across all phase-shifter positions. (6) Polarimetric reconstructions of the Stokes parameters were achieved by using the PSI algorithm to reconstruct the fiber phase, in combination with the dual-scan approach, to minimize channel cross talk. For comparison, the reference-beam calibration was also performed by taking reference data at input polarizer orientation of 22.5 deg, together with the dual-scan approach. It should be noted that we only collected one reference measurement at room temperature for the reference-beam approach. Although, in practice, reference data are collected frequently over a particular interval of time, our goal is to demonstrate that one can avoid this inconvenient step of collecting multiple reference measurements by adopting the PSI method.

#### 4 Experimental Results

This section presents the experimental results of the PSI and reference-beam calibrations at input polarizer orientations of 0 deg and 30 deg, relative to the positive x axis and at fiber's temperatures of 20°C, 35°C, 40°C, 45°C, and 50°C. Figure 5 demonstrates the polarimetric reconstruction results, for both the PSI calibration technique and the reference-beam technique, at an input linear polarization state of 0 deg  $(S_1/S_0 =$ 1 and  $S_2/S_0 = 0$ ). The reconstruction results were collected over the spectral range spanning from 550 to 650 nm, which was limited by the LED's spectral bandwidth full width at half maximum as well as the optical fiber's spectral bandwidth. It can be observed from the reference-beam calibration results in Figs. 5(a) and 5(c) that the Stokes parameters exhibit sinusoidal oscillations as the temperature is increased. This is due to the high temperature dependence of the fiber's birefringence.<sup>27,28</sup> The reference-beam calibration cannot determine or calibrate for the phase retardation but, instead, requires that the sample data are calibrated by

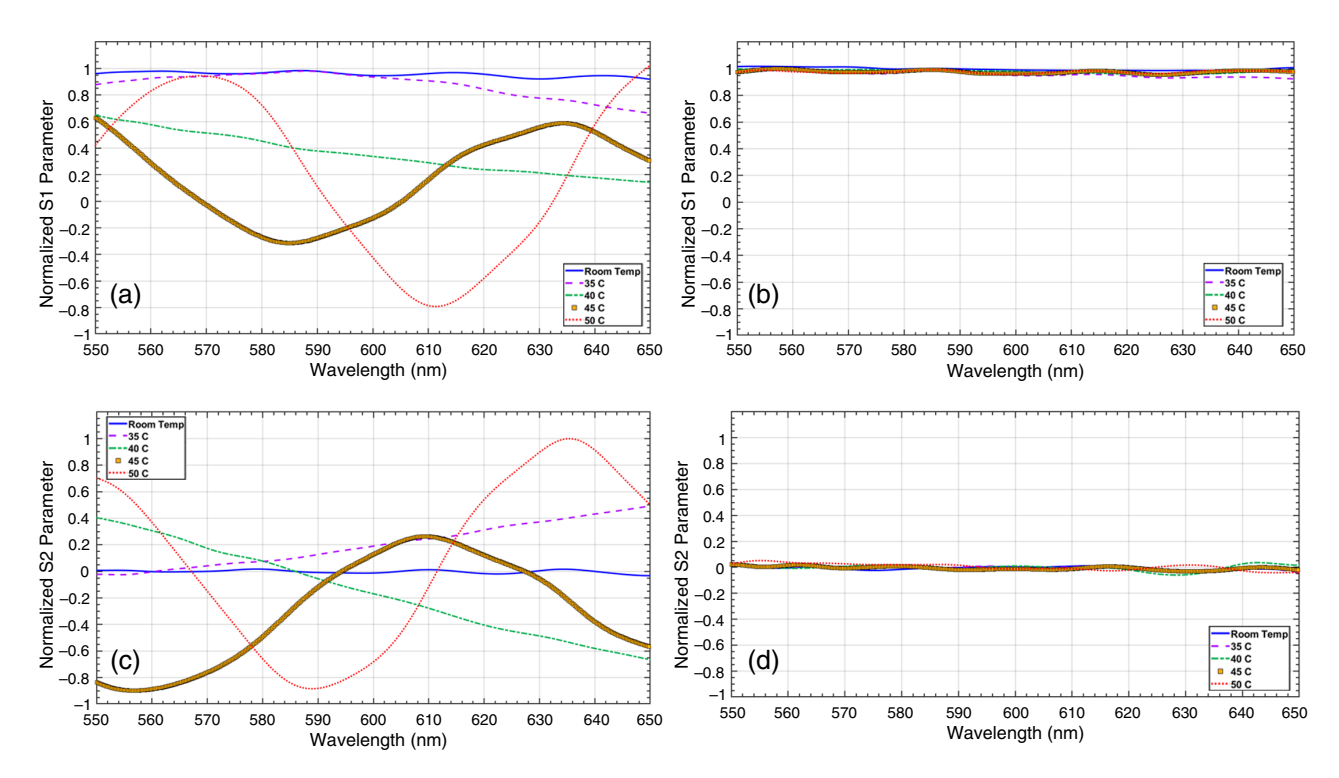


**Fig. 5** Stokes reconstruction results at 0 deg input polarizer: (a)  $S_1$  parameter reconstruction in reference beam, (b)  $S_1$  parameter reconstruction in PSI, (c)  $S_2$  parameter reconstruction in reference beam, and (d)  $S_2$  parameter reconstruction in PSI. The unit of wavelength is nm.

comparison to a set of reference data with a known Stokes parameter distribution. <sup>21</sup> It also assumes that the sample and reference data have equal phase retardations or that the phase changes by the same amount for the sample and the reference data. Consequently, errors occur when the sample data are reconstructed due to uncertainty in the fiber's phase. By contrast, the PSI calibration method can accurately determine and calibrate for the fiber's phase, mitigating these phase-related reconstruction errors. This can be observed from Figs. 5(b) and 5(d) where the reconstructions of  $S_1$  and  $S_2$  are relatively flat and minimally influenced by temperature changes.

To quantify the performance improvement, the root mean square (RMS) error was calculated between the measurements and theoretical values across all temperatures and

**Table 1** RMS errors of the reconstructed Stokes parameters at 0 deg input polarizer for the PSI and reference-beam calibration.

Temperature	S <sub>1</sub> RMS error (%) – PSI	S <sub>2</sub> RMS error (%) – PSI	S <sub>1</sub> RMS error (%) – Ref.	
21	1.1	1.3	3.9	1.7
35	2.5	1.4	15.3	25.7
40	2.6	2.2	66	35.6
45	2.6	1.5	88.5	49
50	4.6	2.6	101	64.6

measured polarization states. Table 1 depicts the RMS error calculations of the normalized Stokes parameters for linear input of 0 deg for both PSI and reference-beam techniques. The results in Table 1 demonstrate that the PSI calibration method offers significantly lower RMS error in the Stokes reconstructions, when compared to the reference-beam method. We also calculated the average RMS error across the different temperatures in Table 1. The average RMS errors of  $S_1$  and  $S_2$ , using the PSI technique, are 2.7% and 1.8%, respectively, whereas the average RMS errors of  $S_1$  and  $S_2$ , using the reference-beam technique, are 54.9% and 35.3%, respectively. This indicates that the PSI method offers an improvement in the reconstruction of  $S_1$  and  $S_2$  by a factor of 20.3 and 19.6, respectively, when compared to the reference-beam calibration.

We also provide the reconstruction results of  $S_1$  and  $S_2$  at input polarization states of 30 deg, with known normalized Stokes parameters of  $S_1/S_0 = 0.5$  and  $S_2/S_0 = 0.866$ , as depicted in Fig. 6. Note again the sinusoidal pattern of the Stokes parameters in the reference-beam reconstruction method, particularly at high temperatures. Moreover, Table 2 provides the RMS error calculations of the normalized Stokes parameters for a linear polarization of 30 deg for both PSI and reference-beam techniques. The average RMS errors of  $S_1$  and  $S_2$  across the five reported temperatures (using the PSI technique) are 1.3% and 1.5%, respectively. In contrast, the average RMS errors of  $S_1$  and  $S_2$ , using the reference-beam technique, are 38.1% and 37.9%, respectively. This shows an improvement in  $S_1$  and  $S_2$  reconstructions by a factor of 29 and 25, respectively, when using the PSI technique.

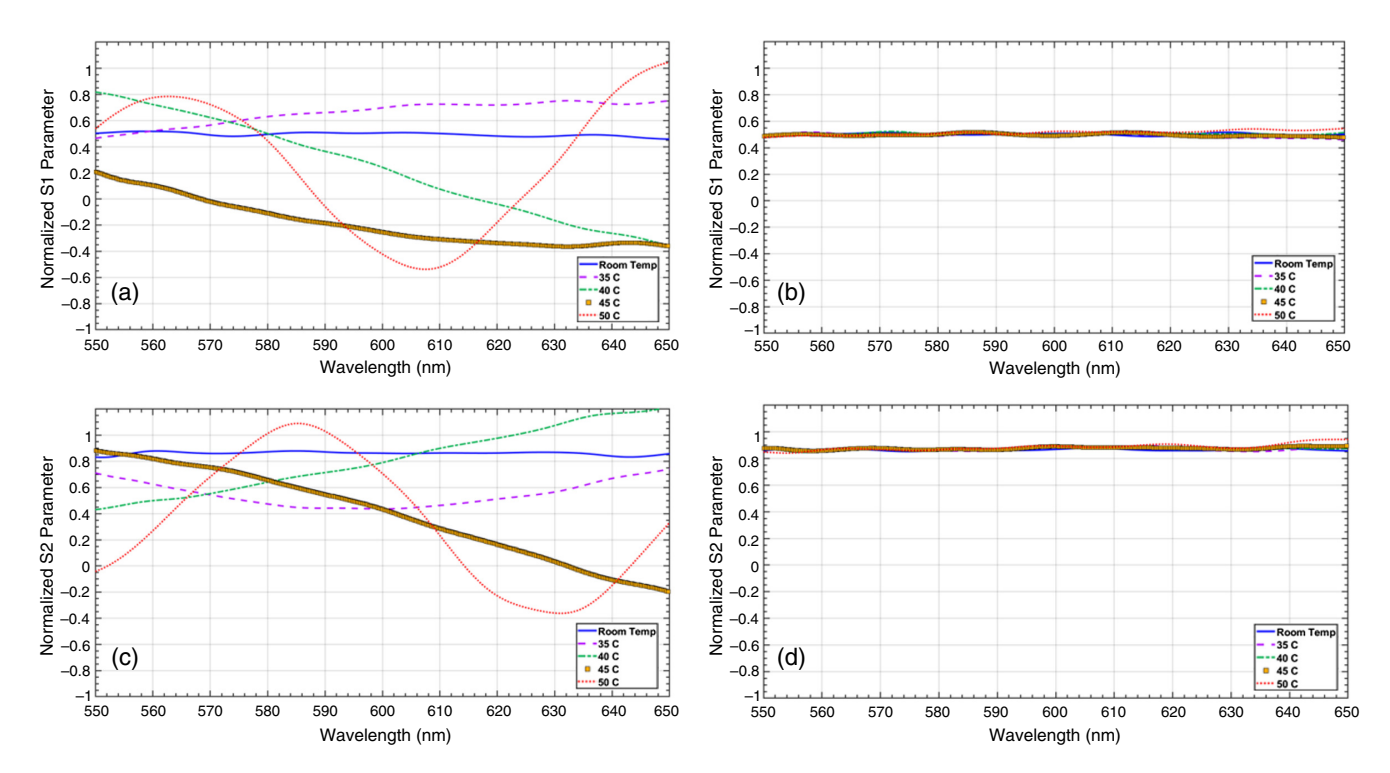


**Fig. 6** Stokes reconstruction results at 30 deg input polarizer: (a)  $S_1$  parameter reconstruction in reference beam, (b)  $S_1$  parameter reconstruction in PSI, (c)  $S_2$  parameter reconstruction in reference beam, and (d)  $S_2$  parameter reconstruction in PSI. The unit of wavelength is nm.

Table 2 RMS errors of the reconstructed Stokes parameters at 30 deg polarizer for the PSI and reference-beam calibrations.

Temperature	S <sub>1</sub> RMS error (%) – PSI	S <sub>2</sub> RMS error (%) – PSI	S <sub>1</sub> RMS error (%) – Ref.	S <sub>2</sub> RMS error (%) – Ref.
21	0.80	0.68	1.54	1.25
35	0.86	1.11	18.2	24.6
40	0.98	1.29	45	33.5
45	1.64	1.41	71	58
50	2.19	3.11	55	72

#### 5 Conclusion

A fiber-based CSP structure that utilizes the PSI calibration technique has been presented. This technique offers high stability and accuracy in the polarimetric reconstruction at different temperatures. A proof of concept of the fiber-based CSP has been experimentally verified. Experimental results show that the PSI calibrations offer higher stability and accuracy in the Stokes reconstructions at different optical fiber temperatures, as compared to the reference-beam calibrations. More specifically, the PSI method offers an improvement in the reconstruction of  $S_1$  and  $S_2$  by a factor of 29 and 25, respectively, when compared to the reference-beam calibration at input polarizer's orientation of 30 deg. These results demonstrate the utility of our proposed technique in that it leads to improved fiber's sensing performance under harsh environmental conditions. Potential advantages can be realized in fiber-based biomedical applications for improved diagnostic performance and in fiber-based MM CSP system for more accurate BRDF measurements.

#### Acknowledgments

This material was based on the work supported by the National Science Foundation under Grant No. 1809753.

#### References

- K. Oka and T. Kato, "Spectroscopic polarimetry with a channeled spectrum," Opt. Lett. 24(21), 1475–1477 (1999).
- 2. F. Snik et al., "An overview of polarimetric sensing techniques and technology with applications to different research fields," Proc. SPIE 9099, 90990B (2014).
- T. Mu et al., "Snapshot linear-Stokes imaging spectropolarimeter using division-of-focal-plane polarimetry and integral field spectroscopy," *Rep.* **7**(1), 42115 (2017).

- Sci. Rep. 7(1), 42115 (2017).
   Z. Wang et al., "Single-shot on-chip spectral sensors based on photonic crystal slabs," Nat. Commun. 10(1), 1020 (2019).
   F. Snik, T. Karalidi, and C. U. Keller, "Spectral modulation for full linear polarimetry," Appl. Opt. 48(7), 1337–1346 (2009).
   F. Snik et al., "A multi-domain full-Stokes polarization modulator that is efficient for 300–2500 nm spectropolarimetry," Proc. SPIE 9613, 26120C (2015) 96130G (2015).
- M. W. Kudenov et al., "Fourier transform channeled spectropolarimetry in the MWIR," *Opt. Express* 15(20), 12792–12805 (2007).
   A. S. Alenin and J. S. Tyo, "Generalized channeled polarimetry," *J. Opt.*
- Soc. Am. A 31(5), 1013–1022 (2014).

- J. Craven-Jones et al., "A thermalized channeled spectropolarimetry using a biaxial potassium titanyl phosphate crystal," *Opt. Lett.* 38(10), 1657–1659 (2013).
- 10. N. Hagen, K. Oka, and E. L. Dereniak, "Snapshot Mueller matrix spectropolarimeter," *Opt. Lett.* **32**(15), 2100–2102 (2007).

  11. S. Manhas et al., "Demonstration of full 4×4 Mueller polarimetry
- through an optical fiber for endoscopic applications," Opt. Express **23**(3), 3047–3054 (2015).
- J. Desroches et al., "Fiber-optic device for endoscopic polarization imaging," *Opt. Lett.* 34(21), 3409–3411 (2009).
   A. Myakov et al., "Fiber optic probe for polarized reflectance spectroscopy in vivo. Design and performance," *J. Biomed. Opt.* 7(3), 388–397
- S. Dargar, "In situ mechanical characterization of multilayer soft tissue using ultrasound imaging," *IEEE Trans. Biomed. Eng.* 64(11), 2595– 2606 (2017).
- 15. Q. Wang et al., "Measurement of internal tissue optical properties at ultraviolet and visible wavelengths: development and implementation of a fiberoptic-based system," *Opt. Express* **16**(12), 8685–8703 (2008).

  16. T. A. Germer and H. J. Patrick, "Mueller matrix bidirectional reflectance
- distribution function measurements and modeling of diffuse reflectance standards," Proc. SPIE 8160, 81600D (2011).
- 17. M. W. Kudenov et al., "Snapshot imaging Mueller matrix polarimeter using polarization gratings," *Opt. Lett.* **37**(8), 1367–1369 (2012).
- 18. F. Zhang and J. W. Lit, "Temperature sensitivity measurements of high-birefringent polarization-maintaining fibers," *Proc. SPIE* **1580**, 450
- 19. E. Kim and T. E. Milner, "Fiber-based single-channel polarizationsensitive spectral interferometry," J. Opt. Soc. Am. A 23(6), 1458–1467
- 20. A. Altaqui and M. W. Kudenov, "Phase-shifting interferometry-based Fourier transform channeled spectropolarimeter," Appl. Opt. 58(7),
- 1830–1840 (2019).

  21. A. Taniguchi et al., "Stabilization of a channeled spectropolarimeter by self-calibration," *Opt. Lett.* 31(22), 3279–3281 (2006).
- 22. D. Goldstein, Polarized Light, 3rd ed., CRC Press, Boca Raton, Florida (2010).
- V. Ramaswamy, W. G. French, and R. D. Standley, "Polarization characteristics of noncircular core single-mode fibers," *Appl. Opt.* 17(18), 3014-3017 (1978).
- 24. M. P. Kothiyal and C. Delisle, "Shearing interferometer for phase shifting interferometry with polarization phase shifter," Appl. Opt. 24(24), 4439–4442 (1985).
- D. Malacara, Optical Shop Testing, 3rd ed., Wiley Series in Pure and Applied Optics, Wiley-Interscience, Hoboken, New Jersey (2007).
- 26. J. Craven, "False signature reduction in channeled spectropolarimetry," Opt. Eng. 49(5), 053602 (2010).

  27. F. Zhang and J. W. Y. Lit, "Temperature and strain sensitivity measure-
- ments of high-birefringent polarization-maintaining fibers," Appl. Opt. **32**(13), 2213–2218 (1993).
- 28. L. Wang et al., "Analysis on stability of polarization-transforming performance of fiber wave plate," Optik 157, 1249-1258 (2018).

Ali Altaqui received his BE degree in telecommunications and his MPhil degree in electrical engineering from the University of Sydney in 2012 and 2014, respectively. Currently, he is a PhD student in electrical engineering at North Carolina State University. He works at the Optical Sensing Lab under the direction of Dr. Michael Kudenov. His research focuses on developing new techniques in channeled spectropolarimetry and organic-based photodetectors for polarization and hyperspectral imaging. Applications include remote sensing, biomedical imaging, food safety, agriculture, and astronomy.

Michael W. Kudenov is an associate professor of electrical and computer engineering at North Carolina State University in Raleigh, North Carolina. He graduated in 2005 from the University of Alaska Fairbanks with a BS degree in electrical engineering and in 2009 from the University of Arizona with a PhD in optical sciences. His research focuses on the development, calibration, and validation of new spectral and polarimetric imaging systems for wavelengths spanning the UV to the thermal IR, including high speed and snapshot imaging spectrometers, polarimeters, cross-correlation spectrometers, and spectropolarimeters. Applications include space situational awareness, chemical imaging, quality control, optical modeling and calibration, agriculture, and phenotyping.